Chapter 9: Understanding Gravity Maps

Abstract

Satellite derived gravity maps for both the moon and earth has become available in recent years, but there is uncertainty as to what the patterns show. They do not reflect the Plate Tectonics model. Looking at recognized craters and crater derived basins on the moon, the gravity patterns are analyzed and those patterns applied to several large ring structures seen in gravity maps of the earth. The best fit for the pattern is obtained when other less visible ring structures are also taken into account. The Teewinot and Bighorn circles in the Rocky Mountains, U.S.A. exemplifies this, producing a comparable pattern to Moscoviense and Freundlich-Sharonov cratering basins on the farside of the moon. This justifies identifying the Teewinot and Bighorn circles as cratering structures.

Introduction

Since their conception, the value of gravity maps has been well accepted for recognizing the structure below the surface of the terrestrial bodies, but what exactly such maps do show has been in questioned. Authors do not agree on how the gravity reading are derived, and therefore what the maps showed. Much of the confusion seems to stem from gravity reading not showing what is expected from a Plate Tectonics Model.

Langlais et al (2010), tried to separate planetary scale magnetic field from the magnetic field generated by the rocks of the crust. While gravity and magnetism are different products they produce similar patterns because magnetic minerals, forms of iron, are commonly the denser lithology and produce higher gravity. Langlais et al determine much of the magnetic distribution suggest a cratering pattern on earth related to the processes that shaped the body during accretion of the planet. They found too many magnetic anomalies to be related to ocean-continental transitions and ocean basins, so plate tectonics is not sufficient to explain the pattern. They suggest it is partly induced by available iron in the crust, but where iron is abundant, minimum magnetism is found. I propose these locations are related to the release wave zones where the adiabatic envelope caused the iron to mineralize separately from the substrate, largely as hematite, a nonmagnetic form. An image of aeromagnetic anomaly map of the Vredefort Structure (Langlais et al 2010) shows a partial circular feature at 10-15 km radius under the high iron amphibolite of the dome, and at 25-30 km radius, in the West Rand Group, an iron rich shale. While they can identify these rings they have no proposal how they fit into a planet size tectonic pattern.

While gravity patterns generally agree with topographic features (Figure 8.11), in some very specific areas, like Bighorn Basin (Figure 9.14), they do not. Colli et al (2016) finds free-air gravity anomaly in some places are too small to adequately account for the topographic changes and in other places are too great to account for the topographic changes. They suggest isostatic roots with low viscosity and convective currents and sublithospheric flow in the mantle to explain some reginal high gravity patterns, but is this necessary?

Steinberger (2016) using the lithospheric thickness model finds many areas where the gravity measurement varies with depth without being supported by topographic changes. Additionally he finds low gravity readings that will not support the topography found there. (Again, the drastic low gravity reading on the Bighorn Basin, Figure 9.14, comes to mind.) Steinberger feels seismic topographic changes (variations in density patterns) in the mantle did support gravity measurements, but they are not always positively associated with the lithosphere's topography. He resorts to viscosity differences and cites supposed age of the mantle to attempt to explain some discrepancies.

Hoggard et al (2017) cites deflection of the earth's surface by convective currents in the mantle to try and explain gravity anomaly patterns. Some of the thinnest crusty underlies depositional basin no matter how high they are piled with sediments. Hoggard et al uses variation in mantle viscosity to provide the upper limits on dynamic topographic. They build this concept on the assumptions that positive and negative gravity anomalies grow and decay over long periods of time and require seismic anomalies moving within the upper mantle generated by temperature changes driving convection currents.

Ebbing et al (2018) recognize a curvature component from bowl shaped domes to bowl shaped basins which they feel needs to be considered when interpreting gravity anomaly reginal patterns. Although they fail to show positive interpretive results, this quality of circular patterns in the data is consistent with Langlies et al (2010) belief that a component of gravity dates back to the origin of the planet by cratering.

Searching for a cratering origin for the surface of the moon and earth, I am suggesting we will recognize ring structures in the gravity patterns left in the lithology and reflected in gravity patterns. If ring structures are recognized by Langlais et al (2010) in the magnetic data, they supports a search for ring structures memorializes in gravity data just as ripple patterns are memorialized in photos of the surface of water. If we can recognize the patterns in a lake, we can use those skills to analyze ripple patterns in gravity on the surface of the moon and earth.

Recognition of Ripple Patterns

The ripple pattern produced by dropping a rock in a pond has much of the same qualities as seen in gravity mapping of impact craters on the moon. The series of ripples produced by the rock's impact on the water's surface moves outwards as a compression/shock wave followed immediately by the expansion/rarefaction/release wave. Because the compression wave produces higher density and expansion wave produces lower density, if the existing lithology captured a "photo" of the compression wave with a slightly higher gravity reading than the following expansion wave, they would generate a bullseye pattern of alternating high and low gravity data.

Figure 9.1 shows an orderly interactions from a series of water drops impacting into a pond. Each impacting drop produced two major rings which can be defined as the original impact ring, as in "6", and a secondary ring produced by the subsequent rebound of the jetting event. Each individual ring consist of two parts, "D" the compression/shock ridge and "E" the expansion/release valley. As these simple rings interact, nodes of cumulative additive energy, "A", develop and cumulative subtractive energy, "B", develop. Trying to locate evidence for impacts that have several layers of later impacts covering them is dependent on locating patterns in these nodes as in ring "5". Although this process is often complicated by wave interactions that break the single expression into a concentric wave-train of smaller expressions as with "C".

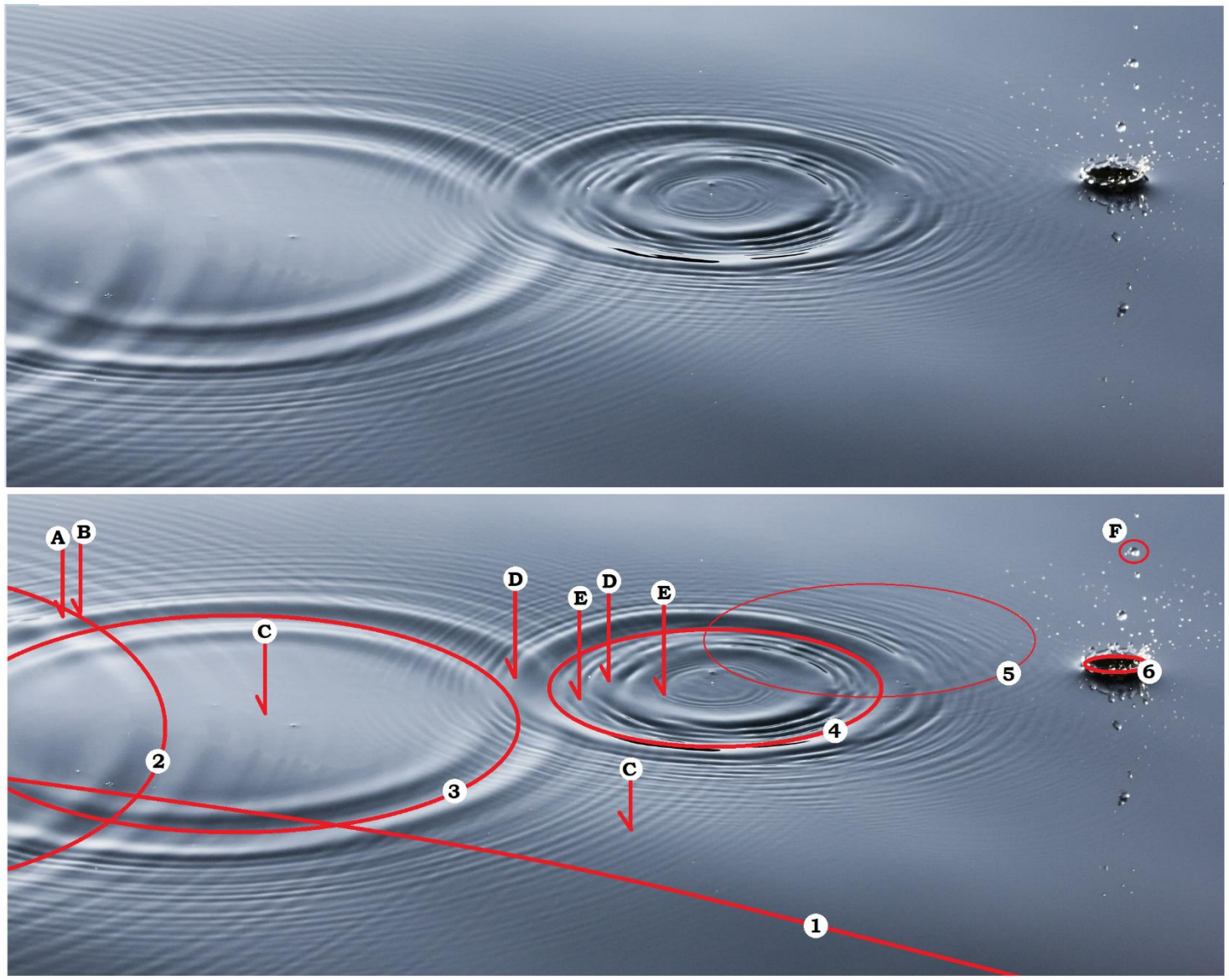

Figure 9.1: Multiple successive impacts in a pond. Numbers represent probable sequence of impacts determined by overlapping patterns of rings. Reader should use extra image to locate defining features of these rings for themselves.

With an increase in impacts the pattern of ripples becomes more complex, Figure 9.2. Yet, even when the numbers of impacts increase, and becomes more disorderly, often at least part of the pattern can be recognized. Ripple set "1" and "2" leave very little evidence in this image. But in a larger view, the node pattern within ring "4" would likely be more obvious over a larger area. This is going to be a significant lesson to look for clues in a larger view, Chapter 2.

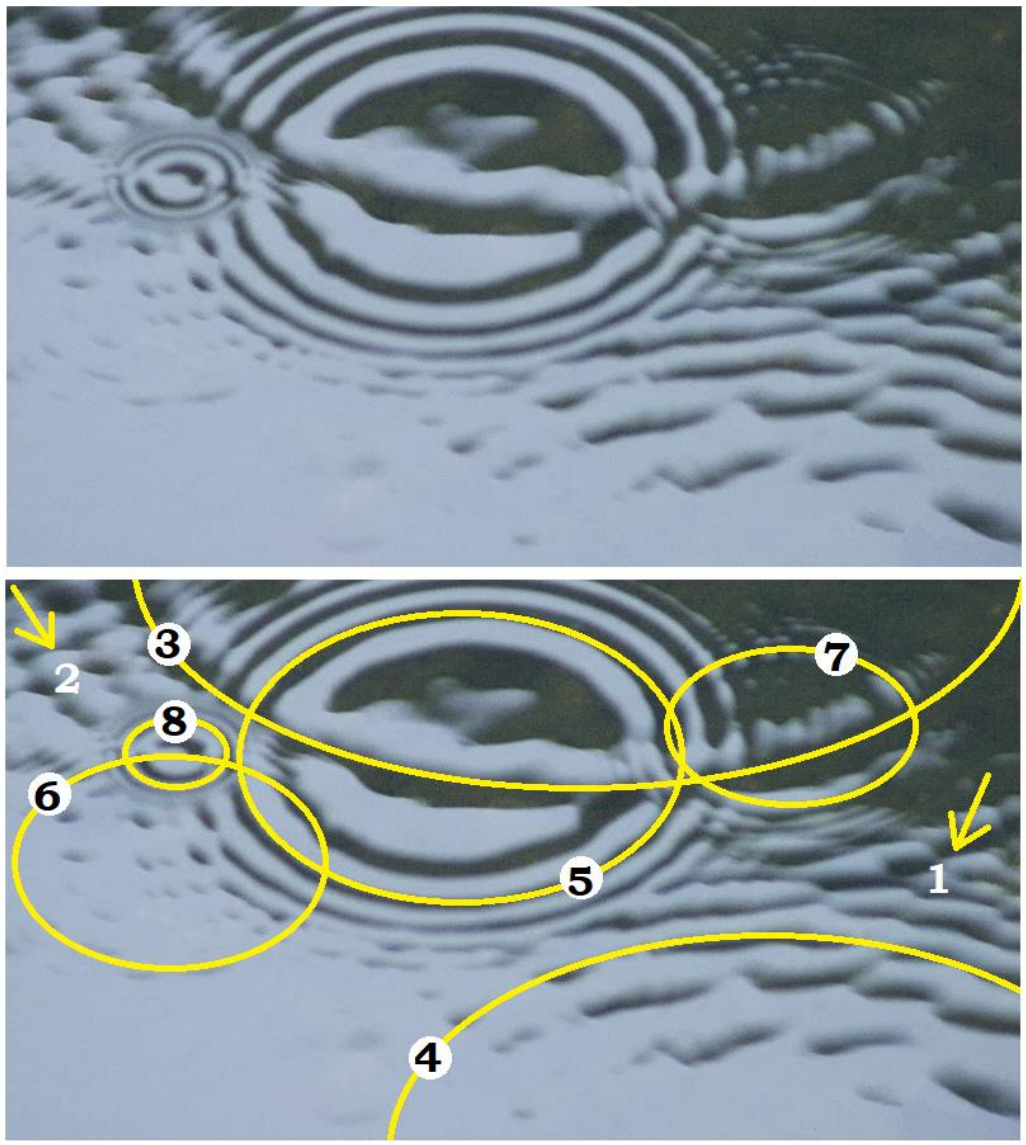

Figure 9.2: An example of less orderly and larger interaction between greater numbers of ripples.

Figure 9.3 is a ripple pattern that is even more disorganized, but defining some of the most obvious rings makes the remaining ones more visible.

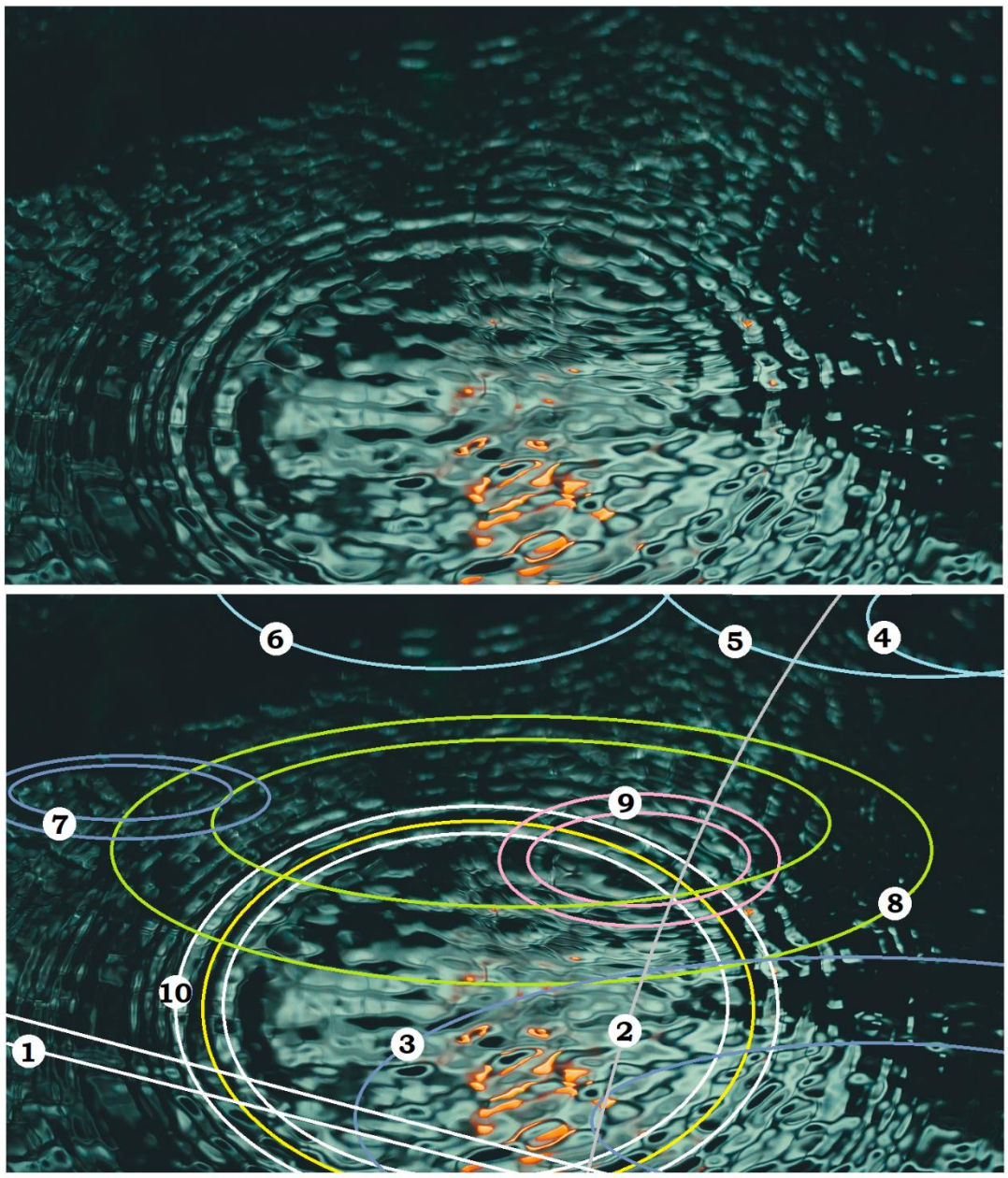

Figure 9.3: A ripple pattern on a pond showing great confusion. All of the rings cannot be discerned but many can, and a larger view would likely reveal more in this same area.

Considering cratering on the moon, maybe we need to compare it to ripples on a pond in a rain storm. As Figure 9.4 demonstrates, even the added energy of rain does not completely obliterate an earlier ripple pattern if it has enough dimension involved with it.

Figure 9.4: Rain on a ripple pattern

Does a superimposed energy pattern obliterate a ripple pattern? This view of a speedboat crossing Lyse fjord suggest it does not. In the engine wake, Figure 9.5B, the number of nods are increased but the pattern of the same five direction is still discernable.

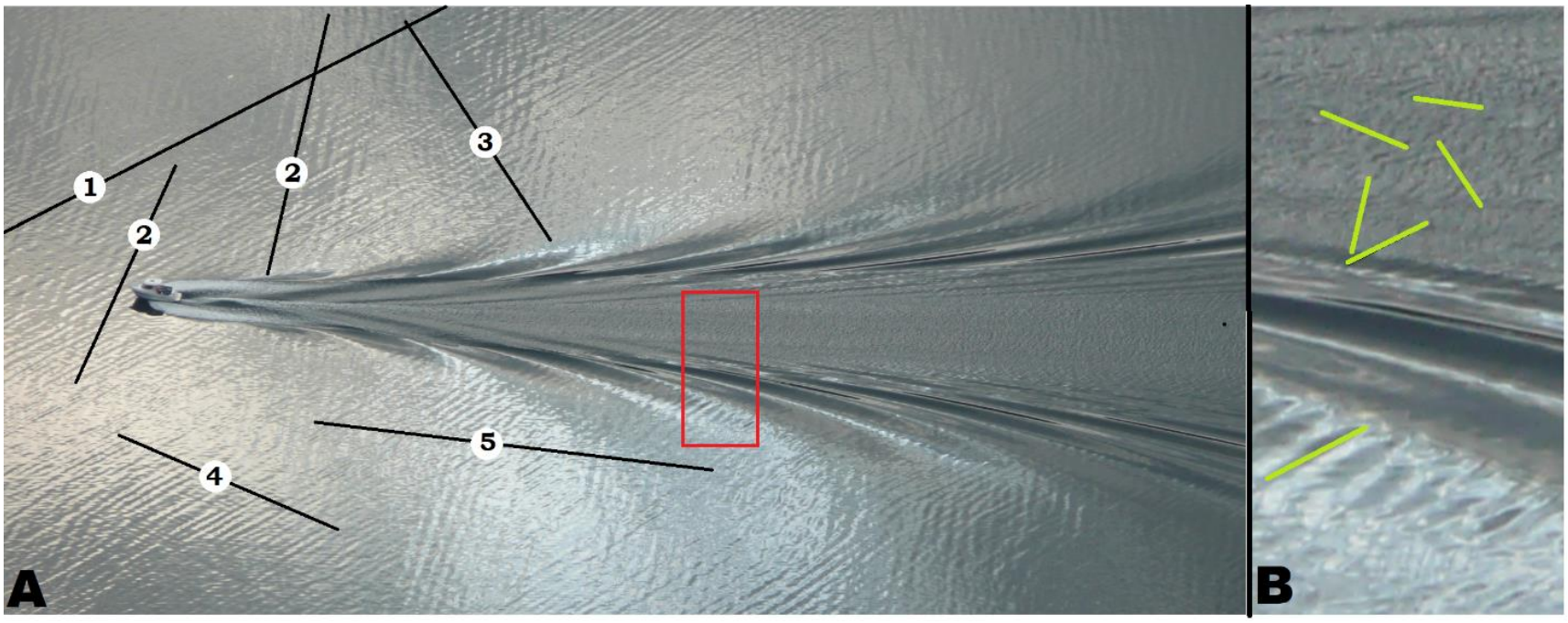

Figure 9.5: Speedboat crossing Lyse fjord, Norway. Five direction of wind wave ripples can be seen around the boat on the fjord, and the same five directions can be seen inside the wake in detail B after the boat engine's energy has been superimposed on it. (Image by Edmont, 4/14/2009.)

While Gravity Maps may not show what some authors expect them to show, they do show circular structures.

Moon's Mare Orientale

The Moon's Mare Orientale is one of the best know circular structures on the moon. Despite its location on the extreme west edge (limb) of the moon, earth bound astronomers using telescopes were readily able to recognize its rings (Hartmann and Kuiper 1962). With satellite imaging it has become one of the most studied large ring structures in our solar system. Despite the discussion of its ring structures, little has been said about its contained lineaments and ghost craters made obvious largely by gravity mapping.

Gravity mapping of the moon was done with a two satellite mission, popularly known as Ebb and Flow, of the Gravity Recovery and Interior Laboratory (GRAIL). It mapped the gravity profile of the lunar surface from the varied attraction of the moon's surface for the individual satellites and resultant slight variation in distance between them. When the GRAIL finds were combined with the Lunar Orbiter Laser Altimeter (LOLA) elevation readings from the Lunar Reconnaissance Orbiter (LRO) of 2009, a much more detailed analysis was obtained.

Figure 9.6A is a GRAIL map overlaid with LOLA elevation data. The image extends beyond the Rocca Ring at 1300-1400 km diameter, the 5th ring Hartmann and Kuiper recognized. Two major linear trends can be seen indicated by the black and white arrow sets. These are the two Concentric Global Ring Structures (CGRSs) that Chapter 10 cites as probably responsible for the Mascon shown by the red in the central circle.

Figure 9.6B, is a detail of Figure 9.6A, but is strictly a gravity map with no indication of elevation. It shows a "bullseye target" form, and the highs and lows extend to the outer annulus which becomes the CGRS. The detail shows smaller indications of the two CGRS, verifying that lineament identification is largely resolution dependent. Figure 9.6B shows also other lineaments both straight and arced, as well as some complete ghost craters, including at least a pair of circles sharing a common center. Chapter 2 showed such nested occurrences of circular lineaments should increase our confidence in recognizing the structure. Examining the dark white circle in Figure 9.6B, the semicircle of 6-8 small rings are noted on the northwest edge. This is highly reminiscent of the erosion pattern on the west edge of Upheaval Dome, a recognized crater structure near Moab, Utah, U.S.A. (Figure 9.7).

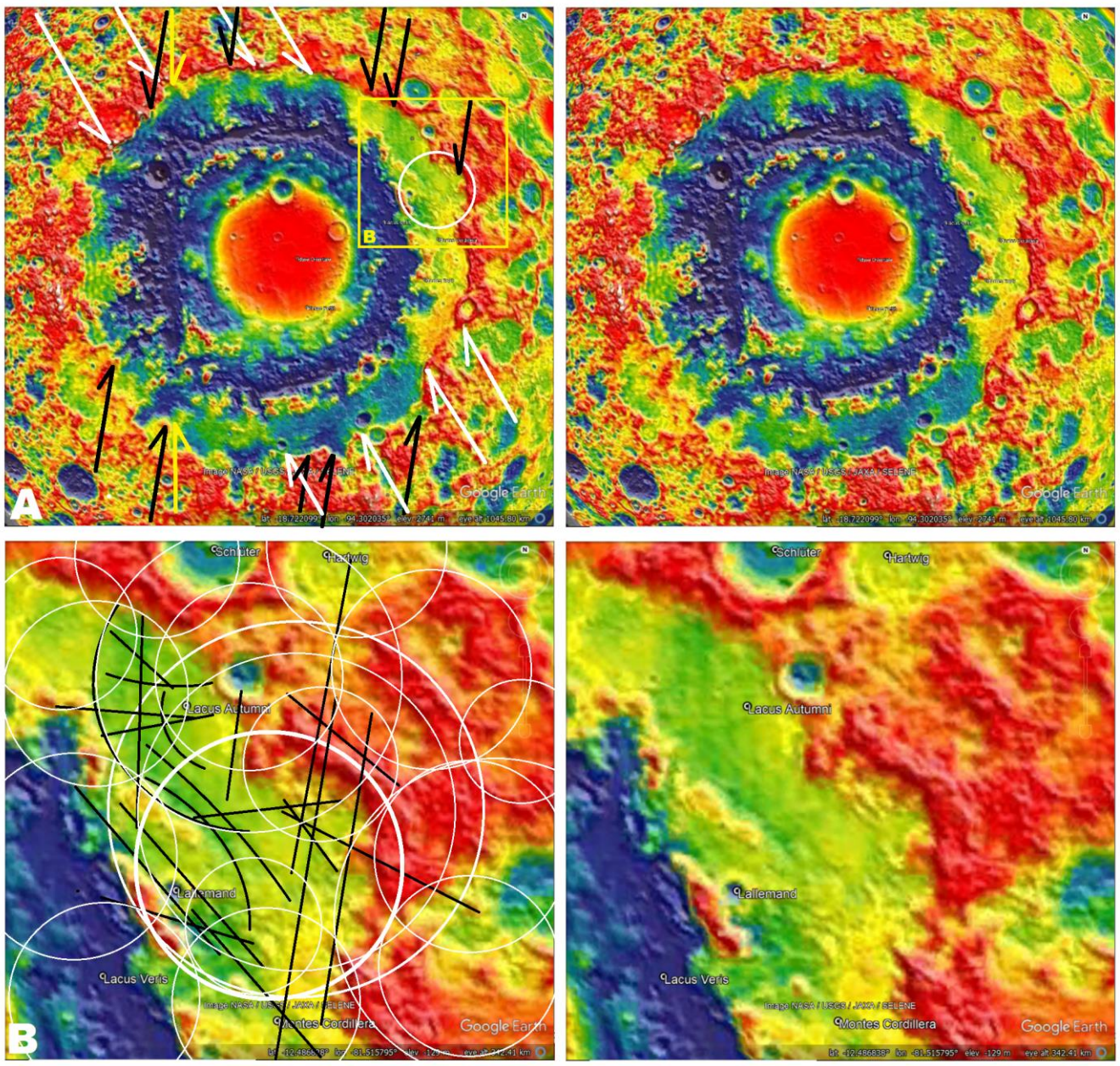

Figure 9.6: Mare Orientale with GRAIL and LOLA data. (A) The entire crater within the OCR-ring. (B) Detail B showing linears and ghost craters visible in gravity patterns. (Image credit: GRAIL.)

Figure 9.7: Upheaval Dome, Utah, from Google Maps. Linears indicate some of the rings of the crater visible in the topography, and some of the smaller erosional ghost craters seen in the immediate environment.

Figure 9.8 shows some of the ghost craters around Mare Orientale which can be recognized in the gravity data. Since most of these craters do not show a mascon, and the Grimaldi and Crüger (Crüger is a <50 km diameter crater included in the mascon) impactors do

not show clear indications of their craters in the gravity pattern, the mascon craters came first, these ghost craters came next, and Mare Orientale crater is probably the last of these larger impacts. The energy of the number “1” crater was still in the lithology when the Mare Orientale impactor struck to form the green area where the two craters overlapped.

Since all of these craters are visible in GRAIL data, it indicates the individual craters produce a distinct energy signature which leave a distinct pattern in gravity mapping.

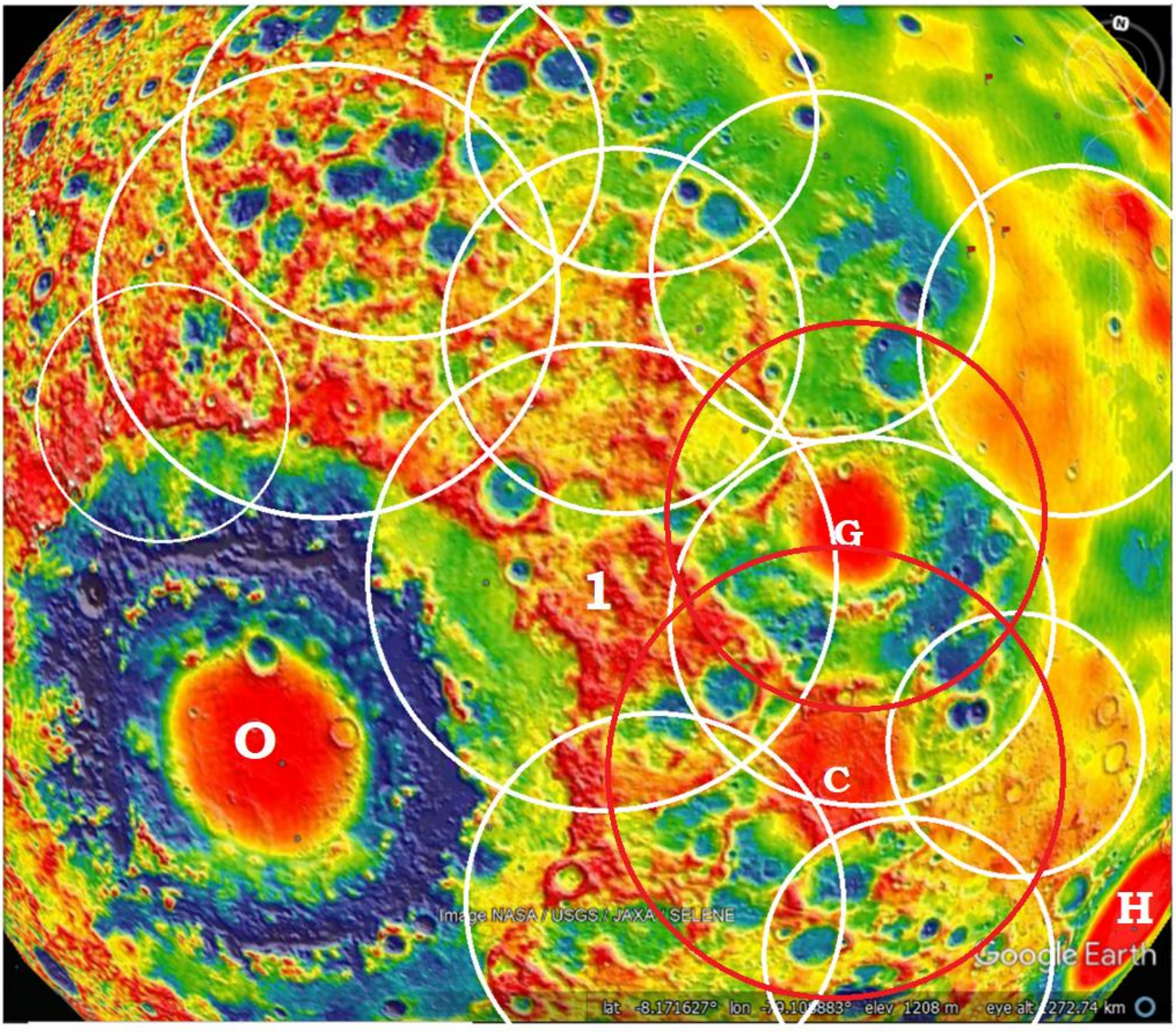

Figure 9.8: Mare Orientale map showing both GRAIL gravity and LOLA elevation data. O = Mare Orientale, H=Mare Humorum. G =Grimaldi, C= Crüger (Not the larger crater, but a small contained crater.)

Moscoviense and Freundlich-Sharonov Basins

Another region of the Moon having a distinct energy pattern in the GRAIL gravity map is around the Moscoviense and Freundlich-Sharonov Basins on the farside of the moon. Immediately around the basins are a bullseye pattern of red and blue concentric ring pattern of high and low gravity readings, Figure 9.9.

And when the area of generally high gravity (red) just north of the Moscoviense and Freundlich-Sharonov Basins is examined, it is not all evenly red, Figure 9.10, but the variations reflect underlying or underlying patterns of other ghost craters. Two distinct CGRS add to that high gravity reading, Figure 9.11, with their center in the Korolev crater. The two blue lines show parallel low gravity linears that follow the CGRS and are created by the release wave in the same manner as the Pacific Fracture Zones, Figure 4.21 and 22, while the shock wave was forming the high gravity linear. Even small craters add to the gravity reading, as Figures 9.10 shows. If their craters show enough variation in the gravity data to map these 10-100 km diameter, they have definitely added to the total expressed gravity.

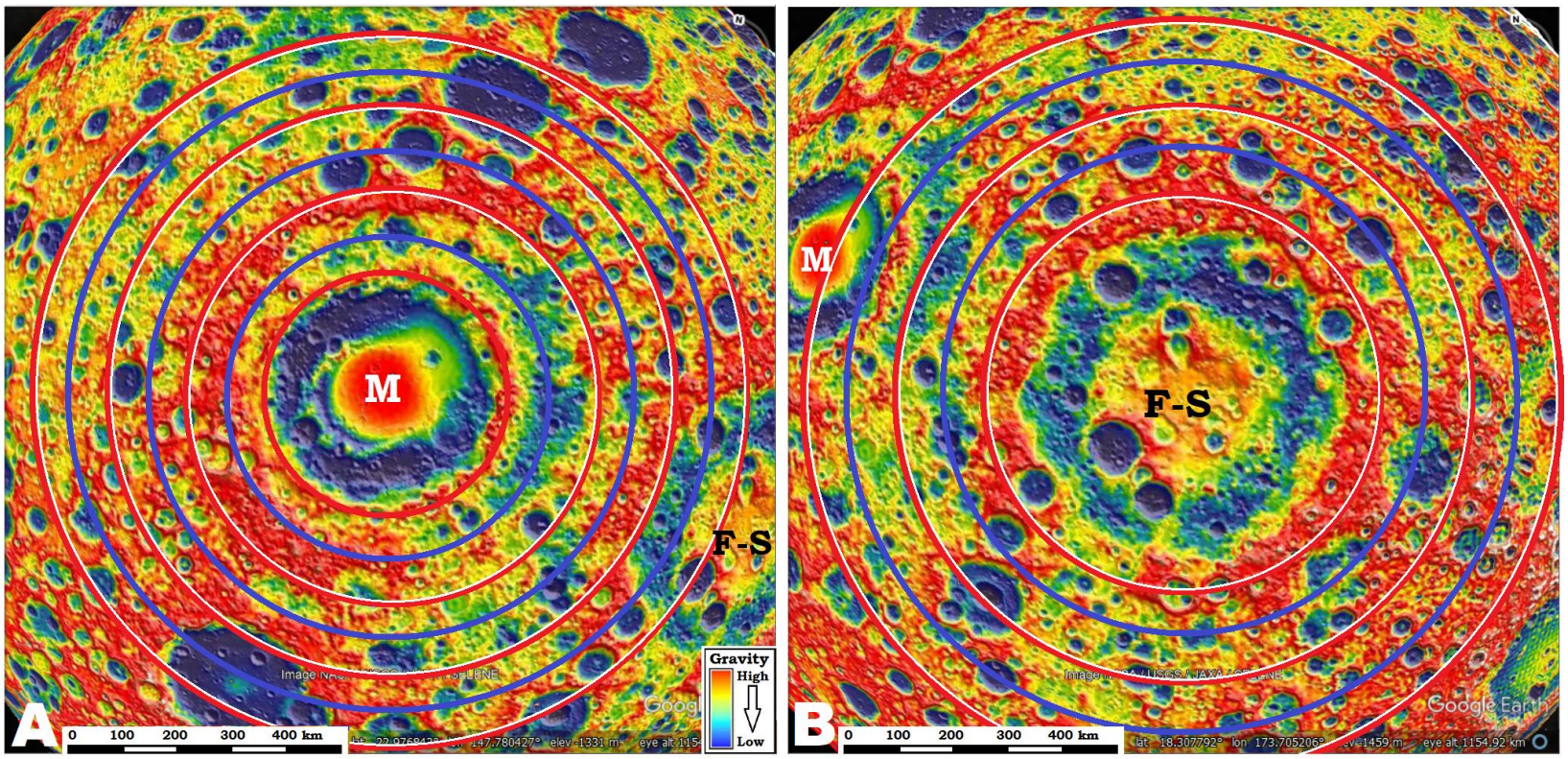

Figure 9.9: Combined GRAIL and LOLA data of A: Moscoviense (M) and B: Freundlich-Sharonov (F-S) Basins.

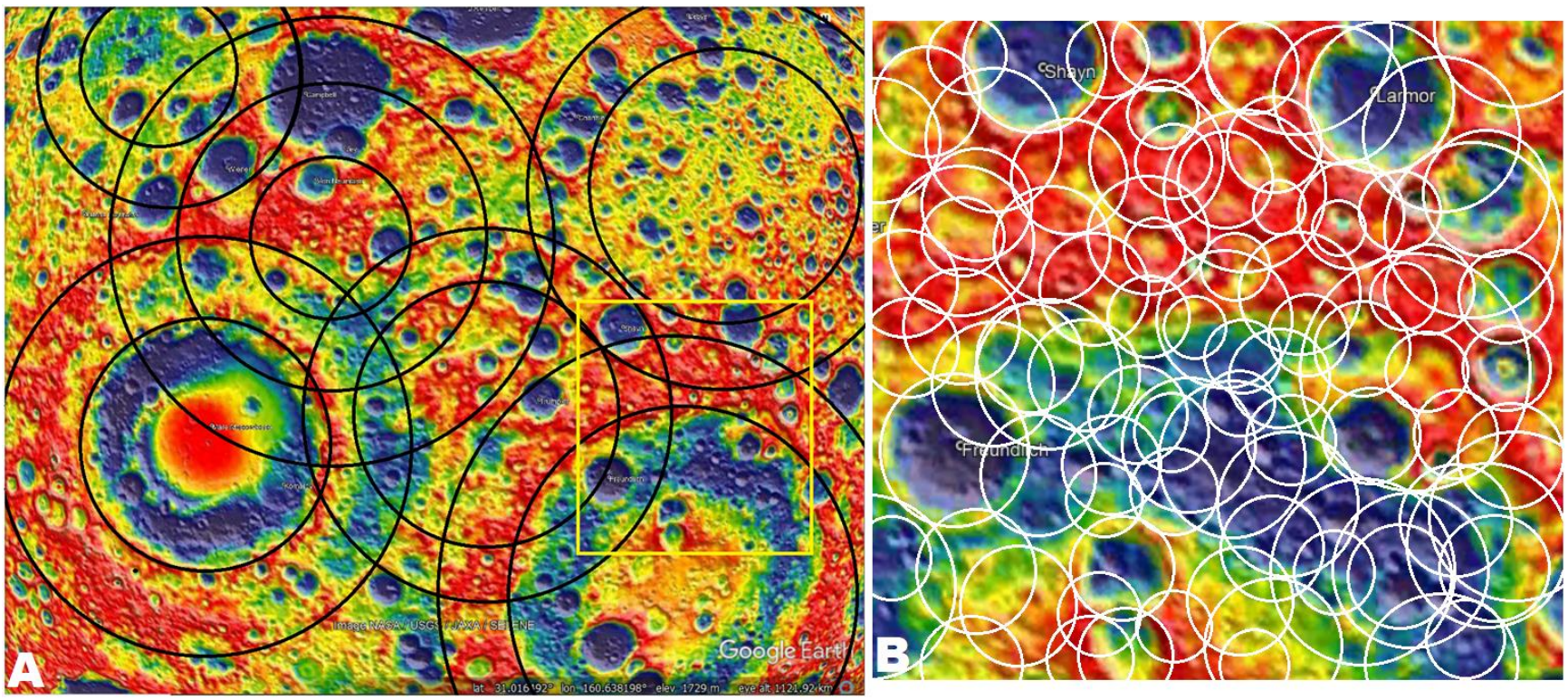

Figure 9.10: GRAIL and LOLA combined data on Google Earth, Moon showing context of the Moscoviense and Freundlich-Sharonov Basins. Yellow box shows location of detail B. B) Detail showing sketched craters between 40-150 km diameters from one small area.

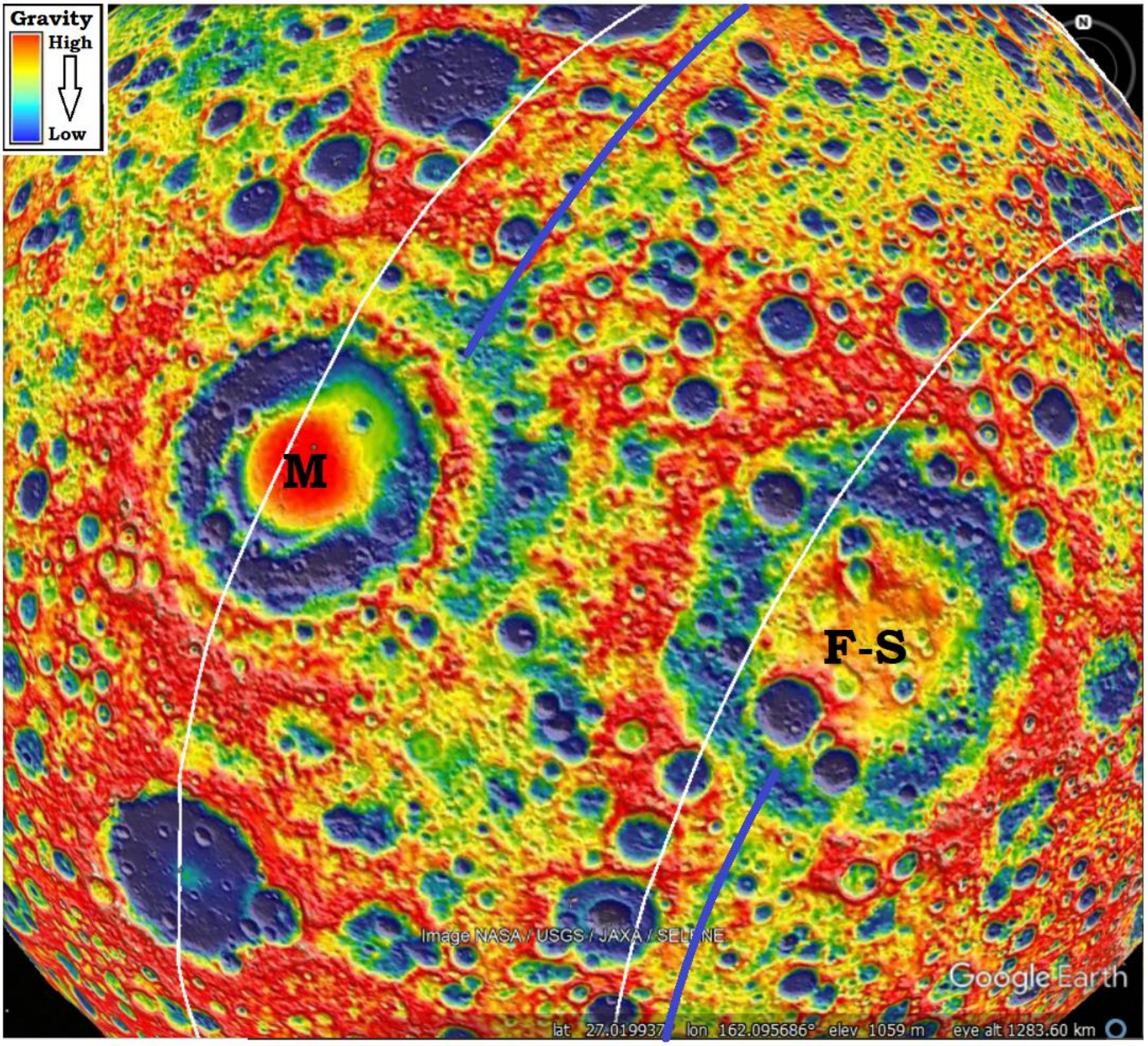

Figure 9.11: Google Earth, Moon image of Moscoviense and Freundlich-Sharonov Basins shown in GRAIL and LOLA data. Concentric circular lineaments center in Korolev crater

Large circular lineaments on Earth

The three most obvious circular lineaments found on earth were introduced in Chapter 2. These are the Mabule crater of southern Africa, the Australia crater which defines the continent of Australia, and the Kara crater in the Kara Sea, north of Siberia. While each of these three ring structures are the most obvious, none of them are complete. Some will say that this incompleteness introduces an aspect of doubt into their validity. I say just the opposite is true. When we can identify other rings and linears that interrupt and partially obscure these craters, the obscured portions verify that they were interacting with similarly sized craters forming at the same time. In Figure 9.12A, the gravity map shows the circle of the Mabule crater is interrupted in the north by the Congo and Zimbabwe craters. Neither of these show up well on the Landsat image, Figure 9.12B. In Figure 9.12C the Australia crater defines the gravity highs around the rim of the continent, but the minable mineral deposits are defined by CGRS from the Caribou crater of western Canada. All of them can be seen much more clearly on the gravity map rather than Landsat, Figure 9.12D.

In Figure 9.12E and F, the Kara crater is at the bottom of the Kara Sea, north of Siberia. The National Oceanic and Atmospheric Administration data is somewhat sparse because it is not on a common shipping lane. The best information for bottom bathymetry is

the Vertical Gravity Gradient derived from satellite altimetry measurements. This is shown in Figure 9.12F. The Vertical Gravity Gradient is greater resolution and detail, but that detail only makes sense viewing it in context with the gravity map to define the crater centers. Actually the Kara crater was found by myself while trying to understand gaps in the rings from the Pacific center and crater discussed in Chapter 3, and represented in black in Figure 9.12E.

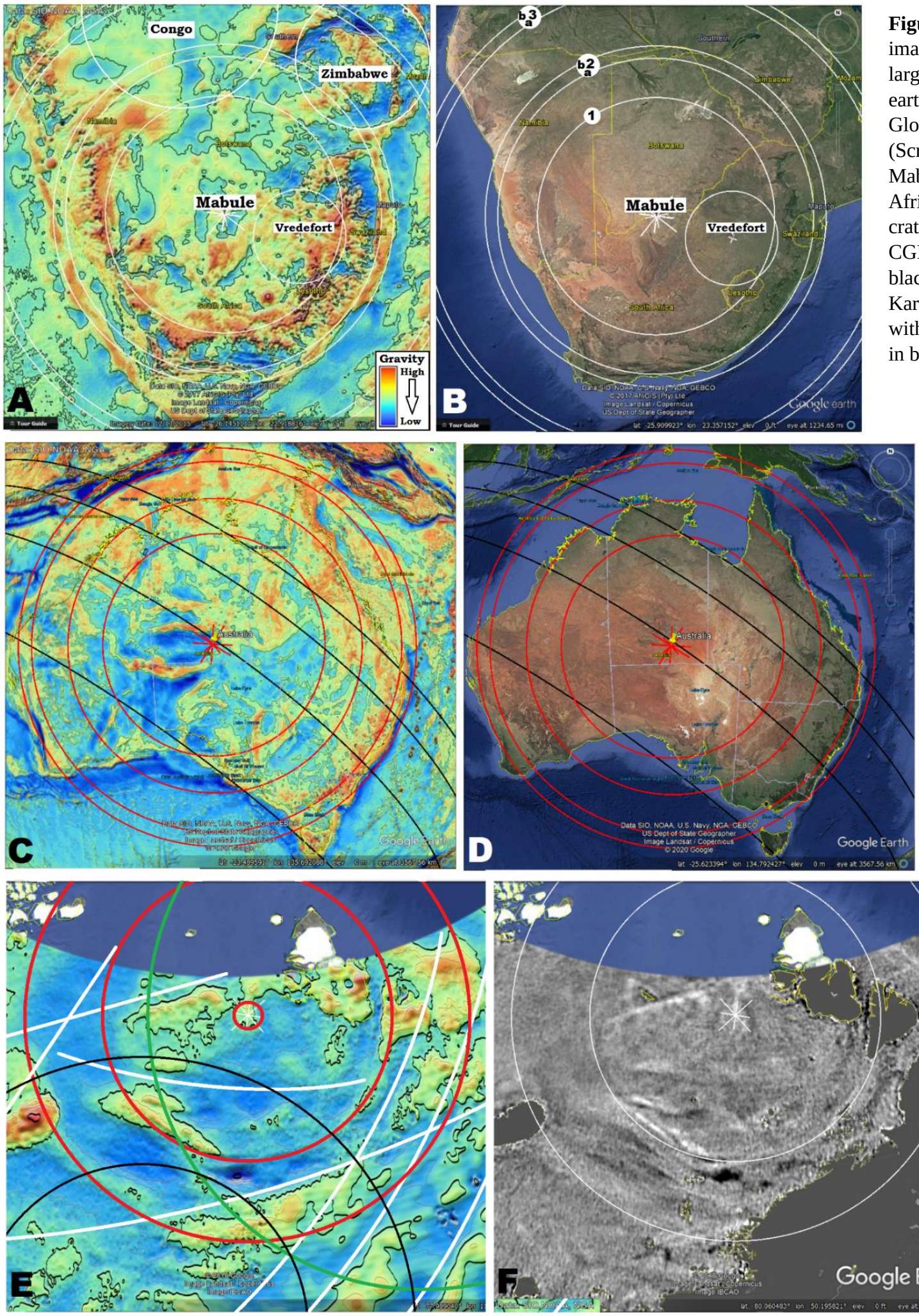

Figure 9.12: Paired images of the three largest, most distinct large earth craters seen in Global Gravity Anomaly (Scripps 2014). A-B: Mabule Crater, southern Africa. C-D: Australia crater, Australia, with CGRS from Caribou in black. E-F: Kara Crater, Kara Sea, north of Siberia with ring of Pacific crater in black.

Comparing the gravity reading of a moon crater with an Earth Crater

Figure 9.9 gives the visual expression of the original distribution of high and low gravity areas in concentric rings around two larger moon craters. The distribution is like the bullseye pattern around the Green River crater, Figures 10.18-19.

Figure 9.13 emphasis the overlap area of Moscoviense and Freundlich-Sharonov basins starting with the mascon (1) in the center with its yellow transition lines, “open rings”, into the dark-blue, release valley (2), of the rest of the crater bowl. The high gravity circle of the OCR ring (3) and release valley (4) between the OCR and the second-ring (5). Once again, comparing the two sets of overlapping circles underlying at least 25 craters with the three most obvious having their OCR-ring indicated in yellow. This is overlapping-ripples-in-a-pond carried to its extreme. But, the primary rings are still adequately distinct to a discerning eye.

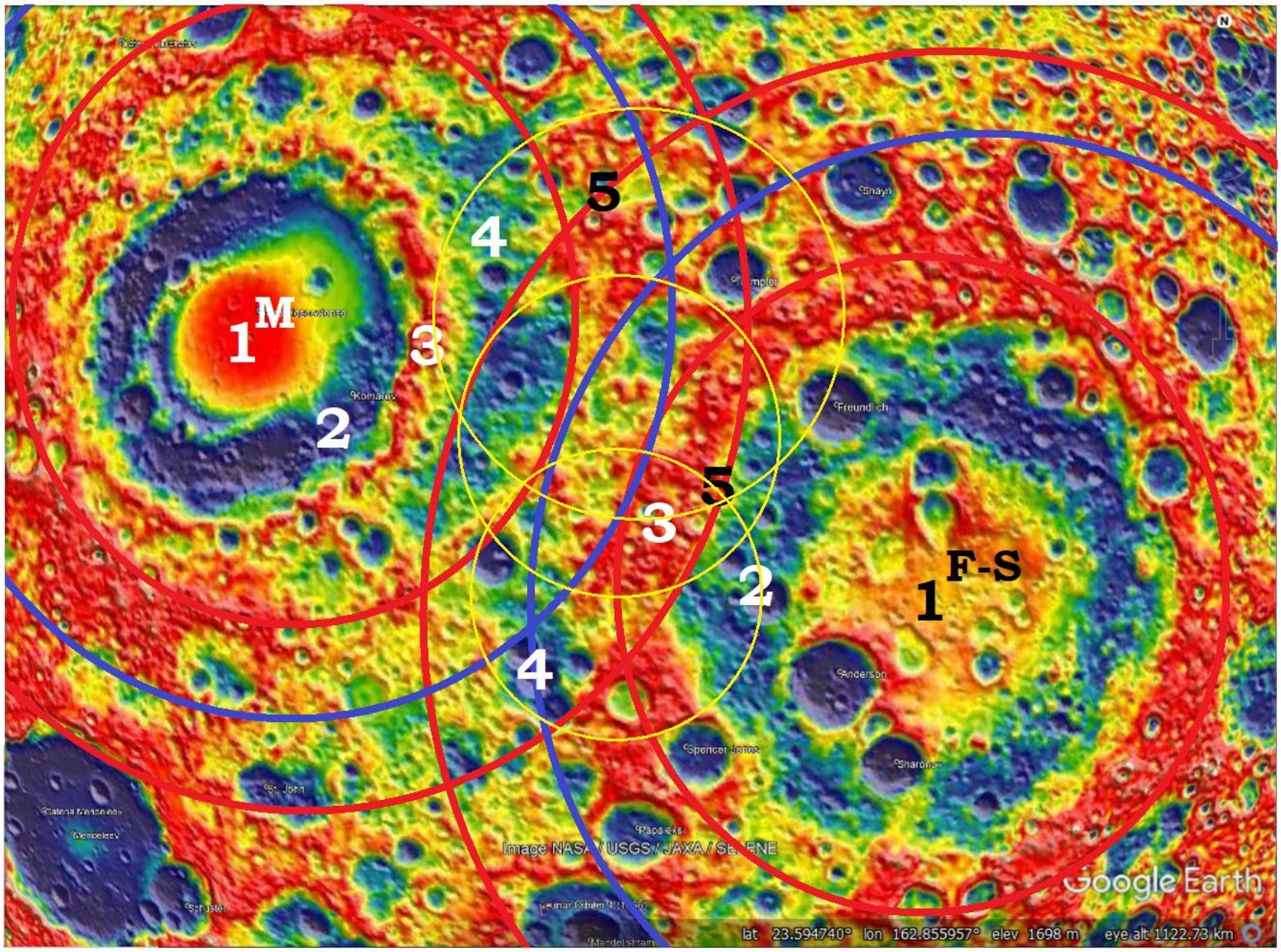

Figure 9.13: Moscoviense (M) and Freundlich-Sharonov (F-S) Basins in GRAIL with LOLA overlay with the Bullseye pattern of high/red gravity readings and low/blue gravity readings as determined in Figure 9.9. Mascon (1) with CGRS expressions, release valley inside OCR (2), OCR ring (3), release valley between OCR and second ring (4), second ring (5).

The normal energy signature of a moon crater, as seen from the GRAIL scan, is very low gravity, dark blue. This is seen beyond the Mascons in both basins as well as on the floor of all of the smaller craters. This is the same low gravity reading of the Bighorn, Wind River, and Powder River Basins, Figure 9.14.

These basins are all high desert plateaus, with significant sedimentary strata cover. So low gravity readings are not reflective of topography. On the moon, the crust is significantly thinned below each large crater, and that may be a source also on Earth. But, it is where the release/ evacuation wave is expressed, forming the expanded sediments/release wave valley.

Yellowstone (5) is a small late crater, in the north-east quadrant of the much larger Teewinot crater. The large white circle is the inner ring of the Teewinot, and the Bighorn Mountains (2) are part of the rim (~650km diameter). The Bighorn Basin (1) and the Wind River Basin (blue area south of it) are part of the low gravity, release-wave valley seen in the comparatively sized Moscoviense Basin

(~400 km diameter rim). While the Yellowstone crater overlays both of these craters, it does not obliterate either one of them and has only slight visibility in gravity, it is visible, reminiscent of overlapping-ripples-on-a-lake.

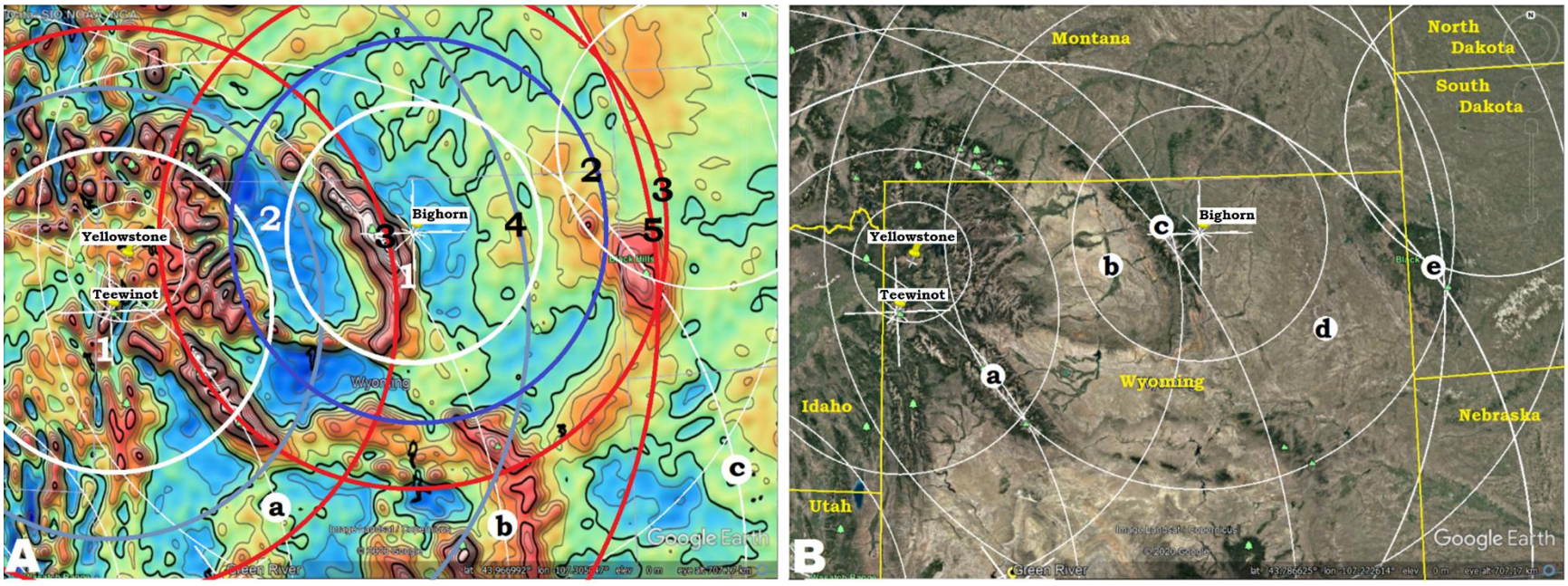

Figure 9.14: Google Earth images of the **Teewinot** and Bighorn craters, through the Black Hills. (A) Global Gravity Anomaly map of the area (Scripps 2014) (B) Same area in Landsat. Gravity map indicating: with heavy white lines "open rings", mascon (1) with CGRS expressions, release valley inside OCR (2), OCR ring (3), release valley between OCR and second ring (4), second ring (5). Linears "a, b, and c" are annulus to Rocky Mountain crater.

Early Heavy Bombardment or Late Heavy Bombardment/ Lunar Cataclysm

Mann 2018 finds that since all returned sample from the Moon have dated at 3.95 Bya (his date for the Late Heavy Bombardment, which in the current model for the Lunar origin), this one date won't work so the Late Heavy Bombardment Cataclysm doesn't work/ didn't happen. Maybe their model doesn't work. They are really saying that all cratering happened within one time period.

Looking at current models for Earth's origin, some secular theorist hold to the earth accreting from planetesmals and meters about 4.55 billion years ago (Allgre and Schneider 2005). As most rock brought back from the moon by Apollo missions date at 4.55 Bya except for samples of lunar basalt that date at 3.16 Bya (Papika et al 1998, this is a different report giving different dates). This has led to the conclusion that the terrestrial bodies had stopped forming by then.

According to a third source, around 3.8 Bya a second bombardment of the terrestrial bodies took place in a Late Heavy Bombardment or Lunar Cataclysm (Redd17). Support for this later episode of impacts has lost favor in some circles in recent years (Mann 2018).

Recognizing the Pacific Fracture Zones as impact structures (CGRS) and their global extent in Chapters 3-5, precludes any major relocation of landmasses after their formation. Additionally, the fossil record contained in sediments that will be shown to be impact derived in the Bighorn and Powder River Basins, as well as the Greater Green River and Rocky Mountain Basins suggest most of the fossil record is connected with this same cratering event. This requires one and only one major cratering episode and I will show it to be connected with the Flood.

Conclusion

So the concept that gravity patterns on the moon and earth show gravity patterns from impact process is a concept that is consistent with the evidence. How this happens will be laid out in the later model, after a little more evidence is gathered by looking at craters below the surface of the crust. Cratering may be a totally new concept for the formation of the surface features for both moon and earth, but it is a concept that is consistent across the entire geologic spectrum if completely understood.

Acknowledgements

Much thanks to Maarten 't Hart who created the overlays for Google Earth Moon for me using cylindrical projection maps of the GRAIL with LOLA, LOLA, and Crustal Thickness map available from NASA at https://svs.gsfc.nasa.gov/4014, accessed April and May 2020.

Reference

Colli, L., S. Ghelichkhan, and H.-P, Bunge. 2016. On the ratio of dynamic topography and gravity anomalies in a dynamic Earth, *Geophysical Research Letters 43*: 2510–2516.

Ebbing, J., P. Haas, F. Ferraccioli, F. Pappa, W. Szwillus, and J. Bouman. 2018. Enhanced satellite gravity gradient imaging, Scientific Reports, Nature.com 8:16356.

GRAIL Map https://svs.gsfc.nasa.gov/4014 accessed 4/25/2020.

Hartmann, W.K. and G.P. Kuiper. 1962. No. 12 Concentric structures surrounding lunar basins, *Communications of the Lunar and Planetary Laboratories* 1:51-66.

Hoggard, M. J., J. Winterbourne, K. Czarnota, and N. White. 2017. Oceanic residual depth measurements, the plate cooling model, and global dynamic topography, *Journal of Geophysical Research: Solid Earth* 122:2328–2372.

Langlais, B., V. Lesur, M.E. Purucker, J.E.P. Connerney, and M. Mandea, 2010. Crustal Magnetic Fields of Terrestrial Planets. *Space Science Review* 152:223-249.

Mann, A. 2018. Cataclysm's end, *Nature* 553: 393-395.

Papike, J., G. Ryder, and Ch. Shearer, 1998. Lunar Samples. *Reviews in Mineralogy and Geochemistry*, 36(5):1-5.234.

Redd, N.T. 2017. The Late Heavy Bombardment; A violent assault on young Earth. https://www.space.com/36661-late-heavy-bombardment.html, accessed 5/13/2020.

Steinberger, B. 2016. Tomography caused by mantle density variations: observation-based estimates and models derived from tomography and lithosphere thickness, *Geophysical Journal International* 205:604-621.